



**HAL**  
open science

## Directional Local Density of States of Classical and Quantum Propagating Surface Plasmons

Martin Berthel, Quanbo Jiang, Aline Pham, Joël Bellessa, Cyriaque Genet,  
Serge Huant, Aurelien Drezet

► **To cite this version:**

Martin Berthel, Quanbo Jiang, Aline Pham, Joël Bellessa, Cyriaque Genet, et al.. Directional Local Density of States of Classical and Quantum Propagating Surface Plasmons. *Physical Review Applied*, 2017, 7 (1), pp.014021. 10.1103/PhysRevApplied.7.014021 . hal-01627769

**HAL Id: hal-01627769**

**<https://hal.science/hal-01627769>**

Submitted on 12 Feb 2021

**HAL** is a multi-disciplinary open access archive for the deposit and dissemination of scientific research documents, whether they are published or not. The documents may come from teaching and research institutions in France or abroad, or from public or private research centers.

L'archive ouverte pluridisciplinaire **HAL**, est destinée au dépôt et à la diffusion de documents scientifiques de niveau recherche, publiés ou non, émanant des établissements d'enseignement et de recherche français ou étrangers, des laboratoires publics ou privés.

# Local Density of States of Classical and Quantum Propagating Surface Plasmons

Martin Berthel,<sup>1</sup> Quanbo Jiang,<sup>1</sup> Aline Pham,<sup>1</sup> Joel Bellessa,<sup>2</sup> Cyriaque Genet,<sup>3</sup> Serge Huant,<sup>1</sup> and Aurélien Drezet<sup>1,\*</sup>

<sup>1</sup>*Institut Néel, CNRS and Université Joseph Fourier, B.P. 166, 38042 Grenoble Cedex, France*

<sup>2</sup>*Institut Lumière Matière, UMR5306 Université Lyon 1-CNRS, Université de Lyon, 69622 Villeurbanne cedex, France*

<sup>3</sup>*ISIS, UMR 7006, CNRS-Université de Strasbourg, 8 allée Monge, 67000 Strasbourg, France*

(Received 25 May 2016; revised manuscript received 10 October 2016)

We theoretically and experimentally introduce the concept of the local density of states (LDOS) associated with propagative surface plasmons (PSPs) launched along a structured thin gold film (a concept we call PSP LDOS). The alternative method couples a near-field optical microscope, in either the classical or the quantum regime of excitation, to a far-field leakage-radiation microscope. This method allows for selecting and collecting a very narrow portion of the directional SP wave vectors, thereby offering sufficient resolution to probe the collimation efficiency of a SP beam for a source near the focal point of a Bragg parabolic reflector. We are able to build and image the PSP LDOS in a fully integrated quantum SP launcher by depositing a diamond nanocrystal hosting nitrogen-vacancy centers at the focal point of the mirror. Our demonstration of the PSP LDOS with quantized SPs offers alternative prospects in the field of quantum plasmonics.

DOI:

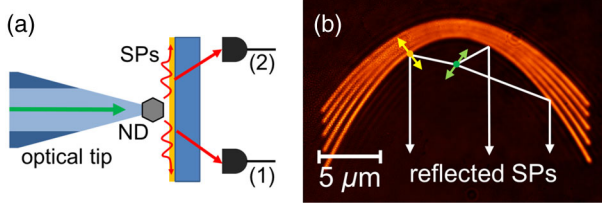
## I. INTRODUCTION

Controlling the emission of a pointlike dipole in a complex environment is a central issue for nanophotonics and nanoplasmonics [1–6]. In this context, the key quantity to be measured is the local density of states (LDOS), which generalizes the concept of the Purcell factor [7]. The LDOS defines the ability of a dipole to populate the various optical modes available in a given environment [8,9]. Since the environment is complex in nanophotonics, both in composition and geometry, the LDOS strongly depends on the dipole location and orientation. This dependence entails the peculiar role played by evanescent waves dressing the objects. In recent years, the photonic LDOS was explored in nanostructures supporting resonant or localized surface plasmon (LSP) modes by means of near-field optical microscopes (NSOMs) [10,11] that allow for an acute position control of a dipolar pointlike tip in the optical near field [12–14]. Alternative powerful methods have been developed to record these LSP-LDOS near-metal nanoparticles [15–18], colloidal-particle networks [19], or single nanoholes [20]. However, to date, no method has been proposed to operate precise studies of propagative SP (PSP) LDOS on extended and nanostructured metal-dielectric planar systems, where propagating SPs are natural information vehicles for photons along micrometers. Since propagative SPs offer a range of technological applications for two-dimensional information transfer, it becomes crucial to define a protocol for recording PSP LDOS. This issue is the first to be considered in this article. Moreover, in

the context of quantum-information processing, one would ultimately like to control and map these PSP LDOS using a quantum fluorescent emitter scanning over the plasmonic system [21]. This knowledge is indeed particularly relevant since current research focuses on the coupling of quantum emitters to metal nanoantennas [10,14], waveguides [1,22], or structured metal films [23,24], for the ultimate purpose of developing fully integrated and optimized single-SP sources. This issue is the second one that we tackle in this work.

In this article, we introduce a general experimental and theoretical scheme for mapping the PSP LDOS in extended and planar devices using a NSOM coupled to resolved back-focal-plane imaging [see Fig. 1(a)]. We demonstrate that this association provides the high contrast and resolution needed for PSP-LDOS measurements. As a second step, we exploit the PSP-LDOS protocol to implement an optimized SP collimator working in the quantum regime. For the purpose of this work, we consider two types of NSOM probes, made of either a classical 100-nm aperture tip or a quantum nitrogen-vacancy- (NV) based optical tip. The latter [25] provides a way to accurately position a single-photon source in a complex environment, spatially limited by the 80-nm nanodiamond that hosts the NVs. Both sorts of tips are placed in the near field of a gold film to convert the light they emit into propagative SPs. In order to map the SP propagation, we use a leakage-radiation microscope (LRM) that records the coupled light transmitted through the thin metal layer in the glass substrate [24,26–31]. Briefly, an elementary SP characterized by its in-plane wave vector  $\mathbf{k}_{\text{SP}}$  leaks into the glass [see Fig. 1(a)] and couples to light of in-plane wave vector  $\mathbf{k}$ , matching the

\*aurelien.drezet@neel.cnrs.fr



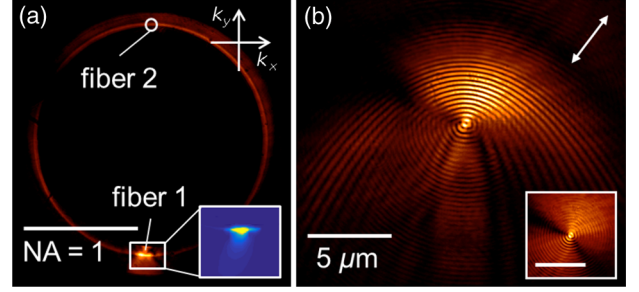
F1:1 FIG. 1. Principle of the experiment. (a) Either a classical-  
 F1:2 aperture NSOM tip (not shown here) or an active NV-based  
 F1:3 NSOM tip excites SPs on a 50-nm-thick gold film evaporated on  
 F1:4 a glass substrate. Leakage radiation of the emitted SPs in the  
 F1:5 Fourier plane (1) in a given direction or (2) collected with a high-  
 F1:6 numerical-aperture (NA) microscope objective. (b) Image of the  
 F1:7 direct plane of the structured gold film in transmission under  
 F1:8 global illumination. Five confocal parabolic slits, each of 150 nm  
 F1:9 width, are milled by a FIB. Most SPs emitted by a dipole located  
 F1:10 at the focus point (the green double arrow) are reflected in the  
 F1:11 same direction by the parabolas' induced dipoles (the yellow  
 F1:12 double arrow), giving a collimated SP beam.

79 real part of  $\mathbf{k}_{\text{SP}}$ . Leaky waves are emitted at the  
 80 fixed angle  $\Theta_{\text{LRM}}$  defined by the condition  $\text{Re}[k_{\text{SP}}] =$   
 81  $(2\pi/\lambda)n_g \sin(\Theta_{\text{LRM}})$  (where  $n_g$  is the glass-substrate optical  
 82 index and  $\lambda$  the optical wavelength). Being a far-field  
 83 method, a LRM is powerful in mapping SP propagation  
 84 over a metal film and has been applied in the context of  
 85 quantum plasmonics, i.e., for the demonstration of single-  
 86 SP launching, a wave-particle-duality test, and a measure-  
 87 ment of second-order temporal and spatial coherence  
 88 [23,32]. Furthermore, the LRM also provides a way for  
 89 determining the plane-wave angular spectrum associated  
 90 with the intensity distribution  $I_{\text{SP}}(\mathbf{k}_{\text{SP}})$  in the Fourier space  
 91 [24,26,29–31]. This approach defines a methodology for  
 92 mapping the PSP LDOS in the  $\mathbf{k}_{\text{SP}}$  space, as demon-  
 93 strated below.

## 94 II. PROOF OF PRINCIPLE

95 The plasmonic device we consider is a Bragg parabolic  
 96 mirror [28] made of five confocal slits (each with a 150 nm  
 97 width) milled using a *focused ion beam* (FIB) in a 50-nm-  
 98 thick gold film. The Bragg condition is such that a pointlike  
 99 source located near the focus excites propagative SPs  
 100 subsequently reflected along the symmetry axis of the  
 101 in-plane mirror. An optical image of the structure recorded  
 102 using a far-field illumination is displayed in Fig. 1(b).

103 Prior to going to the PSP-LDOS measurements, it is  
 104 necessary to interpret the LRM images of the parabolic  
 105 reflector (see also Ref. [32]), first with the classical tip  
 106 used for excitation ( $\lambda_{\text{exc}} = 633$  nm). Typical LRM images  
 107 recorded by a camera capturing the SP propagation in the  
 108 Fourier plane of an oil-immersion objective are displayed in  
 109 Fig. 2(a) and in the direct image plane in Fig. 2(b). The tip  
 110 is located above the metal film (the tip-surface distance is  
 111 kept at  $h \approx 20$  nm) near the parabolas' common focus  $F$ .  
 112 The thin ring observed in the Fourier plane is the typical



F2:1 FIG. 2. LRM images [recorded, respectively, in the (a) Fourier  
 F2:2 and (b) direct planes] with a classical NSOM tip facing the gold  
 F2:3 film at the focus of the parabolas. The inset in (a) is an  
 F2:4 enlargement of the simulation for the Fourier-plane zone col-  
 F2:5 lected by fiber 1. The inset in (b) is a LRM image obtained with  
 F2:6 the same NSOM tip along the plain metal film (500 nm is the  
 F2:7 scale bar for the inset). In (a) NA stands for numerical aperture. In  
 F2:8 (b), a double white arrow indicates the dipole orientation. The  
 F2:9 closest parabola to the focus point  $F$  is represented by a white  
 F2:10 dashed curve.

signature of the leaky SPs launched by the NSOM tip [26].  
 In the direct plane, the 2D profile shows a SP wave  
 generated by an in-plane electric dipole which is also  
 visible in Fig. 2(a) as an anisotropy in the radiation profile.  
 When the tip is positioned at  $F$ , the emitted SPs reflected by  
 the Bragg mirror are strongly collimated along a specific  $\mathbf{k}$   
 direction [see Fig. 2(a)]. The same behavior is observed in  
 the direct-plane image as shown in Fig. 2(b), where several  
 fringes are also superposed to the initial SP wave induced  
 by the NSOM tip for SPs launched by the same NSOM tip  
 on a plain gold film [see the inset of Fig. 2(b)].

18 In order to theoretically describe LRM images, we use a  
 modal expansion into transverse-magnetic (TM) and -  
 electric (TE) waves [24,29]. Considering an oscillating  
 pointlike electric dipole  $\boldsymbol{\mu}e^{-i\omega t}$  (with  $(\omega/c) = (2\pi/\lambda)$ )  
 located at a height  $h$  above the air-gold interface, we  
 express the radiated intensity in the Fourier plane as a  
 function of the in-plane wave vector  $\mathbf{k}$  of the radiated light.  
 Here, the TM term dominates [24,29] and we have

$$I_{\text{TM}}(\mathbf{k}) \approx \eta \left| \frac{\boldsymbol{\mu} \cdot \hat{\mathbf{z}}}{\sqrt{(2\pi/\lambda)^2 - k^2}} - \frac{\boldsymbol{\mu} \cdot \mathbf{k}}{k^2} \right|^2 F_{\text{SP}}(\mathbf{k}), \quad (1)$$

where  $\hat{\mathbf{z}}$  is a unit vector along the  $z$ -optical axis,  $\eta$  is an  
 overall detection efficiency taking into account the trans-  
 mission of the microscope objective, and  $F_{\text{SP}}(\mathbf{k})$  is a  
 resonant SP Lorentzian profile [29]. In order to simulate  
 the Fourier-plane image of Fig. 2(a), we coherently add to  
 the field generated by the NSOM tip the contribution due  
 to the Bragg mirror. We describe this additional term as a  
 sum of  $N$  elementary electric dipoles  $\boldsymbol{\mu}_p$  ( $p = 1, 2, \dots, N$ )  
 obtained by discretizing the parabolic mirrors (the method  
 is explained in Ref. [24]). Each  $\boldsymbol{\mu}_p$  is excited by the SP

142 field  $\mathbf{E}_{\text{SP}}(\mathbf{x}_p, \mathbf{x}_0)$  acting at the dipole location  $\mathbf{x}_p :=$   
 143  $[x_p, y_p, z_p = 0]$ , while the tip is located at  $\mathbf{x}_0 := [x_0, y_0, h]$ .  
 144 We model the coupling between  $\boldsymbol{\mu}_p$  and  $\mathbf{E}_{\text{SP}}(\mathbf{x}_p, \mathbf{x}_0)$  by a  
 145 linear relation  $\boldsymbol{\mu}_p = \xi[\mathbf{E}_{\text{SP}}(\mathbf{x}_p, \mathbf{x}_0) \cdot \hat{\mathbf{n}}_p]\hat{\mathbf{n}}_p$  where  $\xi$  is a  
 146 constant polarizability and  $\hat{\mathbf{n}}_p$  is an in-plane unit vector  
 147 oriented along the normal to the parabola at  $\mathbf{x}_p$ .

148 We present, in the inset of Fig. 2(a), an enlargement of  
 149 the simulated back-focal-plane image [24,29] obtained with  
 150 the tip located at the parabola focus. It is in a very good  
 151 agreement with the experiment.

152 We now turn on to the PSP-LDOS demonstration. The  
 153 **19** principle [32] is sketched in Fig. 1(a). The tip brought in the  
 154 near field of the metallic film shines on SPs, which leak and  
 155 are recorded in the Fourier plane. Subsequently, after  
 156 selecting and detecting only light leaking along a specific  
 157 wave-vector direction, we map the partial PSP LDOS  
 158 associated with this wave vector by scanning the tip while  
 159 maintaining the detection direction fixed in the Fourier  
 160 plane. As shown below, we unambiguously define the  
 161 partial PSP LDOS with a high  $\mathbf{k}$  resolution in the  
 162 Fourier space.

163 For this purpose, it is worth remembering that the full  
 164 LDOS  $\rho_{\text{LDOS}}(\omega, \mathbf{x}_0)$  associated with a dipole  $\boldsymbol{\mu}e^{-i\omega t}$  is  
 165 given by [8,12,33]

$$\rho_{\text{LDOS}}(\omega, \mathbf{x}_0) = \frac{3}{\pi\omega^2|\boldsymbol{\mu}|^2}P(\omega, \mathbf{x}_0), \quad (2)$$

166 where  $P(\omega, \mathbf{x}_0)$  is the total energy rate of the oscillating  
 167 dipole (including radiative and nonradiative exchanges  
 168 with the environment). For a simple two-level quantum  
 169 emitter [33], we have  $P(\omega, \mathbf{x}_0) = \hbar\omega\Gamma(\omega, \mathbf{x}_0)$ , where  $\Gamma$  is  
 170 the full decay rate including dissipation in the metal. As  
 171 the LRM only accounts for radiative SP modes, we  
 172 define the partial PSP LDOS by integrating the radiative  
 173 power along a fraction of the back focal plane intersect-  
 174 ing the SP ring [see Fig. 2(a)]. The partial PSP-LDOS  
 175 measurement is achieved using two motorized 50- $\mu\text{m}$   
 176 multimode fibers placed in the back focal plane of the  
 177 microscope [see also Ref. [32]]. We use these fibers to  
 178 collect a fraction  $\delta P(\omega, \mathbf{k}, \mathbf{x}_0)$  of the Fourier space in the  
 179 area  $\delta^2\mathbf{k}$ . The radius of each fiber represents only a ratio  
 180  $r = 3\%$  of the SP ring radius, meaning that only an  
 181 angular ratio  $r/\pi \approx 1\%$  of the total PSP LDOS is  
 182 recorded. Therefore, this method provides a way to  
 183 experimentally define an angularly resolved PSP LDOS  
 184 with a resolution of 1% (which could be improved by  
 185 reducing the collection-fiber diameter). We define the  
 186 concept of partial PSP LDOS as

$$\delta\rho_{\text{PSP LDOS}}(\omega, \mathbf{k}, \mathbf{x}_0) \approx \frac{3}{\pi\omega^2|\boldsymbol{\mu}|^2}I_{\text{TM}}(\omega, \mathbf{k}, \mathbf{x}_0)\delta^2\mathbf{k}, \quad (3)$$

187 where  $I_{\text{TM}}(\omega, \mathbf{k}, \mathbf{x}_0)$  includes the contributions of the  
 188 NSOM tip and the Bragg mirror and  $\delta^2\mathbf{k} \approx (\omega/c)^2\pi r^2$ .

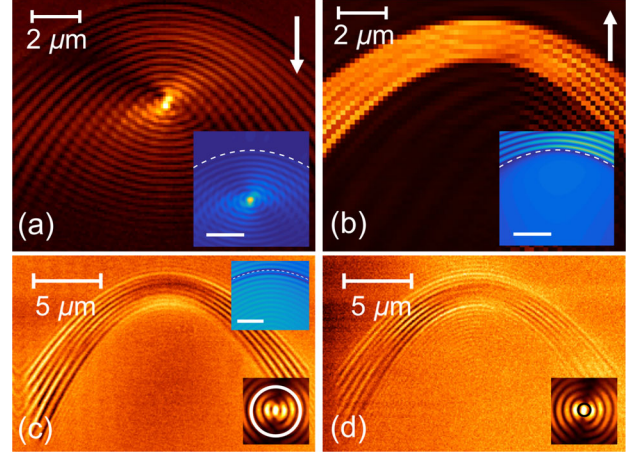
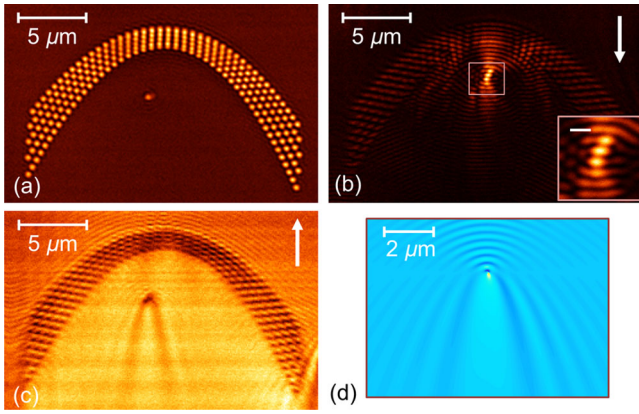


FIG. 3. (a),(b) Experimental partial PSP LDOS of the parabolic structures with an aperture NSOM tip in the classical regime for the collections in regions 1 and 2 of Fig. 2(a), respectively. The white arrow on the top-right corner indicates the collection direction. (Insets) Simulated partial PSP LDOS, scale bar 200 nm. The closest parabola to the focus point is represented by the white dashed curve. (c),(d) Experimental partial PSP LDOS obtained in the direct plane after  $\mathbf{k}$  filtering with a collection fiber of 200 and 50  $\mu\text{m}$  diameter, respectively. The bottom insets in (c) and (d) show a  $\mathbf{k}$ -filtered direct-plane image, with the corresponding collection area, taking into account the X100 magnification of the optical setup. White circle in inset (c), 2  $\mu\text{m}$  diameter; black circle in inset (d), 500 nm diameter. The top inset in (c) is a simulation of the total PSP LDOS.

Partial PSP LDOS associated with two SP directions can be simultaneously recorded by means of the two collection fibers while scanning the tip over the metal film, as illustrated in Figs. 1(a) and 2(a). Figures 3(a) and 3(b) show the PSP-LDOS measurements obtained by scanning the tip over the structure focus and associated with the directions (1) and (2) depicted in Fig. 1(a), i.e., the directions where SPs are strongly reflected or weakly transmitted along the symmetry axis of the parabolas. In Fig. 3(a), a strong contrast near the focus is observed, revealing that  $\delta\rho_{\text{PSP LDOS}}(\omega, \mathbf{k}_1, \mathbf{x}_0)$  is strongly position dependent in this configuration due to the efficient SP collimation occurring with the source near the parabola focus [see Fig. 2(a)]. Conversely,  $\delta\rho_{\text{PSP LDOS}}(\omega, \mathbf{k}_2, \mathbf{x}_0)$  in Fig. 3(b) appears rather flat away from the grooves and does not depend on  $\mathbf{x}_0$ , in agreement with the fact that no SP collimation occurs in direction (2) [see Fig. 2(a)].

Theoretical maps of  $\delta\rho_{\text{SP LDOS}}(\omega, \mathbf{k}_1, \mathbf{x}_0)$  and  $\delta\rho_{\text{SP LDOS}}(\omega, \mathbf{k}_2, \mathbf{x}_0)$  are depicted in the insets of Figs. 3(a) and 3(b), respectively. For simplification, we modeled only one parabolic slit. The main features for each direction are very well reproduced by the simulations.  $\delta\rho_{\text{SP LDOS}}(\omega, \mathbf{k}_1, \mathbf{x}_0)$  features a maximum of intensity localized at the focus point of the parabola surrounded by fringes, while  $\delta\rho_{\text{SP LDOS}}(\omega, \mathbf{k}_2, \mathbf{x}_0)$  remains flat, in agreement with the experimental images.



F4:1 FIG. 4. (a) Unfiltered direct plane NSOM and (b),(c) partial  
 F4:2 PSP-LDOS images of discretized slits forming a parabolic Bragg  
 F4:3 mirror that includes a nanometric defect near the focus point. The  
 F4:4 right arrow in the top-right corner in (b),(c) indicates the  
 F4:5 collection direction. [Inset in (b)] Enlargement of the focus  
 F4:6 point, scale bar 500 nm. (d) Simulation of PSP-LDOS images  
 F4:7 (c) with the nanohole only.

215 A similar experiment is performed with discretized  
 216 parabolas made of milled nanoholes (with the diameter  
 217  $d = 200$  nm). The separation between adjacent holes in a  
 218 given parabola is fixed at  $\lambda_{\text{SPP}}$ . We show in Fig. 4(a) a  
 219 transmission image when the aperture tip is located at  
 220 500 nm of the surface. We observe a defect in the metal  
 221 forming a single nanohole near the focus point of the  
 222 parabolas. Figures 4(b) and 4(c) present the partial PSP-  
 223 LDOS measurements obtained by recording downward and  
 224 upward plasmons, respectively. We see, in the first case,  
 225 the same features as for the continuous parabolas of Fig. 3, i.e.,  
 226 a bright spot on the focus point, demonstrating that SPs are  
 227 strongly reflected by the structure in the downward  
 228 direction. Moreover, the effect of this collimation is so  
 229 intense that the defect has no influence at all. Looking at the  
 230 second partial PSP-LDOS measurement in Fig. 4(c), we  
 231 see, as with the continuous parabolas, a rather flat evolution  
 232 of the intensity. However, we can additionally observe an  
 233 effect of the nanohole, demonstrating a kind of “hyperbolic  
 234 shadowing” that results from interference between different  
 235 SP contributions. The partial PSP LDOS of such a nano-  
 236 hole, approximated as a single dipole, has been simulated  
 237 using the analytical method presented before. The resulting  
 238 calculated image is shown in Fig. 4(d). The qualitative  
 239 features—i.e., the hyperbolic shadowing—observed in  
 240 Fig. 4(c) are again reproduced by our model.

241 Moreover, the above experiments can be analyzed using  
 242 Lorentz’s reciprocity theorem [34], which helps us to  
 243 understand the images features. Indeed, this theorem has  
 244 been intensively studied in the case of electromagnetic  
 245 waves [34–36]. It plays a central role in nano-optics to  
 246 describe and connect various NSOM and LDOS measure-  
 247 ments [14,35,36]. In our case, the tip radially excites SPs  
 248 which can be reflected by the structures. While the structure

249 is scanned, the SPs emitted and reflected along one precise  
 250 direction are collected. Applying the reciprocity theorem to  
 251 this measurement amounts to exciting the structure with a  
 252 (nearly perfect) plasmonic plane wave, coming from the  
 253 actual collection direction. Finally, to complete the reci-  
 254 procity, we have to imagine a NSOM tip in the detection  
 255 mode that probes the plasmonic field above the chosen area.  
 256 For parabolas, the plane wave would excite dipoles all  
 257 along the slits, themselves exciting waves that would  
 258 constructively interfere at the focus point. If we could scan  
 259 a NSOM tip in detection mode over this area, we should  
 260 obtain images very similar to what is measured in PSP  
 261 LDOS (a problem which was recently analyzed using a  
 262 NSOM in the detection mode [37]). For a single-hole  
 263 structure, we would have a plane wave that excites a single  
 264 dipole, creating a circular wave. The interference pattern  
 265 obtained between a plane wave and a circular wave is  
 266 typically the one obtained in Figs. 4(c) and 4(d), showing  
 267 that the reciprocity theorem can be applied in this case.

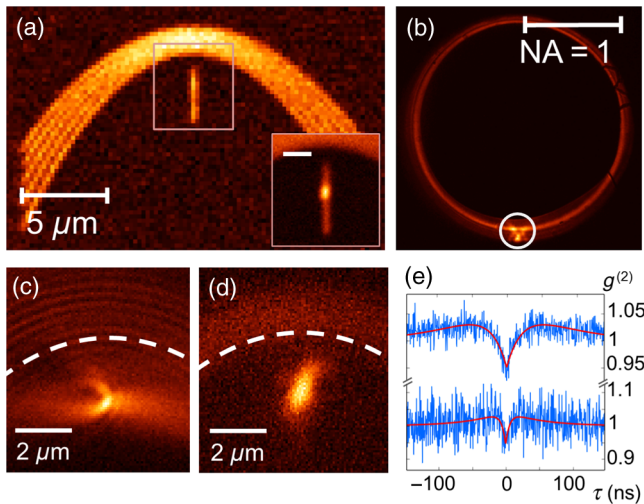
268 It is worth emphasizing that previous LDOS measure-  
 269 ments using NSOMs mapped the full spectrum of radiative  
 270 components emitted by the tip [9,10,13,14], sometimes  
 271 after filtering to keep only the “forbidden” light compo-  
 272 nents [8,9,11,26,27]. Here, however, the issue is to reach  
 273 enough resolution in the Fourier plane to define and map  
 274 properly the partial PSP LDOS associated with specific  
 275 wave vectors  $\mathbf{k}$ . Reaching sufficient resolution is essential  
 276 for our method to be able to select a restricted part of the  
 277 SP ring in order to map the PSP LDOS near the parabola  
 278 focus with a very good resolution. To confirm this belief, 21  
 279 we implement a forbidden light-LDOS measurement by  
 280 mapping in the direct plane the total intensity emitted by the  
 281 tip and using a  $\mathbf{k}$  filter in the Fourier plane that removes  
 282 components corresponding to  $\text{NA} < 1$ . Figures 3(c)  
 283 and 3(d) show two such LDOS maps obtained with two  
 284 different collection-fiber diameters. The rather flat signal  
 285 confirms, in agreement with the theory [see the inset of  
 286 Fig. 3(c)], that integration and averaging over the different  
 287 available SP channels cancel the LDOS sensitivity to the tip  
 288 position and demonstrate that the  $\mathbf{k}$  resolution considered  
 289 in Figs. 3(a) and 3(b) is crucial for successful PSP-LDOS  
 290 mapping.

291 The above experiments have a simple physical inter-  
 292 pretation, and what we show is that there is actually no  
 293 backaction from the reflected plasmons on the excitation  
 294 dipole, whatever its position. This absence of backaction 22  
 295 is indeed critical for the PSP-LDOS measurement since  
 296 the PSP LDOS is defined for a fixed-dipole moment. Clearly,  
 297 this assumption would not be correct if the tip  
 298 were near the slits. However, for points near the focus,  
 299 which are relevant here, we expect that the tip is not too  
 300 disturbed by the structure. Here, the SP signal reflected by 23  
 301 the mirror and coming back on the tip could affect, in turn,  
 302 the tip emission, and this situation is monitored in our  
 303 experiment by detecting photons emitted near the tip

304 [see Figs. 3(c) and 3(d)]. The collection fiber conjugated  
 305 with the sample plane discriminates against those useful  
 306 photons from the background and those coming from the  
 307 structure. Here, the collection fiber is represented by a  
 308 circular collection area centered on the dipole. The  
 309 measurement has been done with a 200- $\mu\text{m}$  (50- $\mu\text{m}$ )  
 310 collection fiber, shown in Fig. 3(c) [Fig. 3(d)]. The inset  
 311 in each figure shows the collection area, taking into  
 312 account the magnification of the setup, compared to the  
 313 filtered direct-plane image of the tip. In both cases, we see  
 314 that the signal remains nearly constant when the tip is far  
 315 away from the slit, apart from very slight modulations.  
 316 Therefore, the emitting power of the tip is unchanged  
 317 when we scan the structure, including in the region of  
 318 **24** interest, i.e., around the focus point.

### 319 III. APPLICATION IN THE QUANTUM REGIME

320 **25** We now are in position to turn on to the quantum regime  
 321 of SP excitation. We show in Fig. 5(c) the corresponding  
 322 PSP-LDOS measurement with the NV-based probe excited  
 323 at 532 nm, revealing the same features as in Fig. 3(b). We  
 324 emphasize that the concept of PSP LDOS remains valid in  
 325 the quantum regime. Indeed, above an area far from the  
 326 slits, the effective dipole associated with the tip is not  
 327 significantly disturbed by the SP-reflected field and there-  
 328 **26** fore remains independent of its position. This result is



F5:1 FIG. 5. Deposition of the ND at the focus point of confocal  
 F5:2 parabolas. (a) NSOM image with the tip retracted (500 nm), with  
 F5:3 a ND hosting 17 NV centers. The parabolas are the same as they  
 F5:4 were previously, but with an additional 4- $\mu\text{m}$ -long slit milled  
 F5:5 through the focus point. (Inset) The ND is deposited on the slit.  
 F5:6 Scale bar, 2  $\mu\text{m}$ . (b) Fourier-plane image when the deposited ND  
 F5:7 is excited. Scale bar, 2  $\mu\text{m}$ . (c) Experimental quantum partial SP LDOS of the  
 F5:8 parabolas without an additional slit with the NV-based tip.  
 F5:9 (d) Scan on the structure with the deposited ND while collecting  
 F5:10 the Fourier plane in the area marked by the white circle in (b).  
 F5:11 (e)  $g^{(2)}(\tau)$  functions of the ND (top chart) above glass and  
 F5:12 (bottom chart) after a dropoff in gold.

329 confirmed by Fig. 3(d), which shows that the NSOM tip  
 330 intensity remains constant along the plane surface, i.e., far  
 331 from the slits. Moreover, for the quantum system, the NVs  
 332 used as quantum emitters are in a saturation regime so that  
 333 the emitted power remains constant [21].

334 An elaborated configuration is implemented in the  
 335 quantum regime to be able to measure the quantum  
 336 correlation function  $g^{(2)}(\tau)$  when the ND is located at  
 337 the focus point above gold. The signal being very weak in  
 338 the previous configuration, acquiring a  $g^{(2)}(\tau)$  function by  
 339 leaving the NV-based tip in a near-field height above the  
 340 focus point for hours would be very challenging. Therefore,  
 341 we directly deposit the ND at the focus point to excite it  
 342 with the tip from the far field. The precise dropoff of the  
 343 ND is assisted by a supplementary slit 4  $\mu\text{m}$  long and  
 344 150 nm wide passing through the focal point and aligned  
 345 with the parabola axis. Figure 5(a) presents a scan of this  
 346 structure with the active tip retracted to the far field. With  
 347 this tip, we catch a ND hosting  $17 \pm 1$  NV centers [top  
 348 chart of Fig. 5(e):  $g^{(2)}(\tau)$  acquired above glass, showing an  
 349 antibunching] and then release it at the focus point [the  
 350 inset of Fig. 5(a) shows a zoom of the slit containing the  
 351 ND after deposition].

352 In the Fourier plane image of Fig. 5(b), we still observe a  
 353 strong SP collimation in the downward direction. The  
 354 pattern here looks different, showing that the ND is slightly  
 355 shifted away from the focus point [see the inset of  
 356 Fig. 5(a)]. However, we are able to collect a large part  
 357 of the collimated signal with a 200- $\mu\text{m}$ -core collection fiber  
 358 [the white circle in Fig. 5(b)]. The signal is strong enough  
 359 to allow for a  $g^{(2)}(\tau)$  measurement [the bottom chart of  
 360 Fig. 5(e)]. An antibunching dip is seen, confirming that the  
 361 quantum signature of the NVs has been conserved after the  
 362 plasmonic propagation [22,23]. By scanning the structure  
 363 in this configuration, we see in Fig. 5(d) a bright spot when  
 364 the ND is excited. By fitting the  $g^{(2)}(\tau)$  curves with a three-  
 365 level model [38], we can extract the intrinsic photophysical  
 366 parameters. The quantum efficiency  $Q$  on the glass is  $Q_g =$   
 367 0.40 and increases to  $Q_f = 0.63$  when the ND is located at  
 368 the focus point. Therefore, the metallic structure has a  
 369 strong effect on the emitter photodynamics [1,32,39].

### 370 IV. CONCLUSIONS AND PERSPECTIVES

371 In this article, we introduce the concept of PSP LDOS. In  
 372 analogy with its previously demonstrated capability of  
 373 imaging LSP LDOS in confined corrals [11], we propose  
 374 an effective way to map the PSP LDOS of a parabolic  
 375 Bragg collimator by means of a NSOM and a  $\mathbf{k}$ -resolved  
 376 LRM. Our scheme is tractable on any planar structure on a  
 377 thin metal film. Using a quantum emitter and the very high  
 378 contrast and resolution of our method, we are able to  
 379 measure the quantum PSP LDOS and the correlation  
 380 function  $g^{(2)}(\tau)$ , and to build a fully integrated quantum  
 381 plasmonic collimator by controlling the deposition of

382 quantum emitters near the focus of the structure, where  
 383 the PSP LDOS reaches its maximum. It is worth noting  
 384 that this quantum plasmonic device is excitable in the  
 385 far field using a laser source, thereby paving the way for  
 386 many applications in the bottom-up development and  
 387 optimization of quantum integrated devices involving  
 388 SPs and quantum emitters. For instance, in addition to  
 389 be well suited to probe the photodynamics of quantum  
 390 emitters coupled to plasmonics systems, this method  
 391 could definitely be useful in the frame of plasmon  
 392 entanglement studies [40,41] and quantum nanophotonic  
 393 circuitry [1,22,42].

### ACKNOWLEDGMENTS

394  
 395 **27** This work was supported by Agence Nationale de la  
 396 Recherche (ANR), France, through SINPHONIE Grant  
 397 No. ANR-12-NANO-0019 and PLACORE Grant  
 398 No. ANR-13-BS10-0007. C.G. also thanks the ANR  
 399 Equipex “Union” (Grant No. ANR-10-EQPX-52-01). The  
 400 Ph.D. grants of A. P., by the Ministère de l’enseignement et  
 401 la recherche, scientifique, and of Q. Jiang, by the Région  
 402 Rhône-Alpes, are gratefully acknowledged. We thank J.-F.  
 403 Motte and G. Julie, from the NANOFAB facility in Neel  
 404 Institute, for sample and NSOM tip fabrication. The nano-  
 405 diamond sample was provided by G. Dantelle and T. Gacoin.

406

- 408 [1] A. V. Akimov, A. Mukherjee, C. L. Yu, D. E. Chang,  
 409 A. S. Zibrov, P. R. Hemmer, H. Park, and M. D. Lukin,  
 410 Generation of single optical plasmons in metallic  
 411 nanowires coupled to quantum dots, *Nature (London)*  
 412 **28** *450*, 402 (2007).  
 413 [2] P. Lodahl, A. F. Van Driel, I. S. Nikolaev, A. Irman, K.  
 414 Obergaag, D. Vanmaekelbergh, and W. L. Vos, Controlling  
 415 the dynamics of spontaneous emission from quantum dots  
 416 by photonic crystals, *Nature (London)* **430**, 654 (2004).  
 417 [3] P. Anger, P. Bharadwaj, and L. Novotny, Enhancement and  
 418 Quenching of Single-Molecule Fluorescence, *Phys. Rev.*  
 419 **29** *Lett.* **96**, 113002 (2006).  
 420 [4] S. Kühn, U. Håkanson, L. Rogobete, and V. Sandoghdar,  
 421 Enhancement of Single-Molecule Fluorescence Using a  
 422 Gold Nanoparticle as an Optical Nanoantenna, *Phys. Rev.*  
 423 *Lett.* **97**, 017402 (2006).  
 424 [5] A. Schietinger, M. Barth, T. Aichele, and O. Benson,  
 425 Plasmon-enhanced single photon emission from a nano-  
 426 assembled metal-diamond hybrid structure at room temper-  
 427 ature, *Nano Lett.* **9**, 1694 (2009).  
 428 [6] M. Frimmer and F. Koenderink, Spontaneous Emission  
 429 Control in a Tunable Hybrid Photonic System, *Phys. Rev.*  
 430 *Lett.* **110**, 217405 (2013).  
 431 **30** [7] G. Colas des Francs, C. Girard, and A. Dereux, Theory of  
 432 near-field optical imaging with a single molecule as light  
 433 source, *J. Chem. Phys.* **117**, 4659 (2002).  
 434 [8] G. Colas des Francs, C. Girard, J. C. Weber, C. Chicane,  
 435 T. David, A. Dereux, and D. Peyrade, Optical Analogy to

- Electronic Quantum Corrals, *Phys. Rev. Lett.* **86**, 4950  
 (2001). 436  
 437  
 [9] C. Chicanne, T. David, R. Quidant, J. C. Weber, Y. Lacroute,  
 438 E. Bourillot, A. Dereux, G. Colas des Francs, and C. Girard,  
 439 Imaging the Local Density of States of Optical Corrals,  
 440 *Phys. Rev. Lett.* **88**, 097402 (2002). 441  
 442  
 [10] L. Aigouy, A. Cazé, P. Gredin, M. Mortier, and R.  
 443 Carminati, Mapping and Quantifying Electric and Magnetic  
 444 Dipole Luminescence at the Nanoscale, *Phys. Rev. Lett.*  
 445 **113**, 076101 (2014). 446  
 447  
 [11] G. Colas des Francs, C. Girard, J. C. Weeber, and A.  
 448 Dereux, Relationship between scanning near-field optical  
 449 images and local density of photonic states, *Chem. Phys.*  
 450 *Lett.* **345**, 512 (2001). 451  
 452  
 [12] R. Carminati, A. Cazé, D. Cao, F. Peragut, V. Krachmalnic-  
 453 off, R. Pierrat, and Y. De Wilde, Electromagnetic density of  
 454 states in complex plasmonic systems, *Surf. Sci. Rep.* **70**, 1  
 455 (2015). 456  
 457  
 [13] V. Krachmalnicoff, D. Cao, A. Cazé, E. Castanié, R. Pierrat,  
 458 N. Bardou, S. Collin, R. Carminati, and Y. De Wilde,  
 459 Towards a full characterization of a plasmonic nanostructure  
 460 with a fluorescent near-field probe, *Opt. Express* **21**, 11536  
 461 (2013). 462  
 463  
 [14] D. Cao, A. Cazé, M. Calabrese, R. Pierrat, N. Bardou, S.  
 464 Collin, R. Carminati, V. Krachmalnicoff, and Y. De Wilde,  
 465 Mapping the radiative and the apparent nonradiative local  
 466 density of states in the near field of a metallic nanoantenna,  
 467 *ACS Photonics* **2**, 189 (2015). 468  
 469  
 [15] K. Imura, T. Nagahara, and H. Okamoto, Near-field two-  
 470 photon-induced photoluminescence from single gold nano-  
 471 rods and imaging of plasmon modes, *J. Phys. Chem. B* **109**,  
 472 13214 (2005). 473  
 474  
 [16] F. J. Garcia de Abajo and M. Kociak, Probing the Photonic  
 475 Local Density of States with Electron Energy Loss Spec-  
 476 troscopy, *Phys. Rev. Lett.* **100**, 106804 (2008). 477  
 478  
 [17] M. Kuttge, E. J. R. Vesseur, A. F. Koenderink, H. J. Lezec,  
 479 H. A. Atwater, F. J. Garcia de Abajo, and A. Polman, Local  
 480 density of states, spectrum, and far-field interference of  
 481 surface plasmon polaritons probed by cathodolumines-  
 482 cence, *Phys. Rev. B* **79**, 113405 (2009). 483  
 484  
 [18] S. Viarbitskaya, A. Teulle, R. Marty, J. Sharma, C. Girard,  
 485 A. Arbouet, and E. Dujardin, Tailoring and imaging the  
 486 plasmonic local density of states in crystalline nanoprisms,  
 487 *Nat. Mater.* **12**, 426 (2013). 488  
 489  
 [19] A. Teulle, M. Bosman, C. Girard, K. L. Gurunatha, M. Li, S.  
 490 Mann, and E. Dujardin, Multimodal plasmonics in fused  
 491 colloidal networks, *Nat. Mater.* **14**, 87 (2014). 492  
 493  
 [20] T. Coenen and A. Polman, Optical properties of single  
 494 plasmonic holes probed with local electron beam excitation,  
 495 *ACS Nano* **8**, 7350 (2014). 496  
 497  
 [21] C. Girard, O. Martin, G. Lévêque, G. Colas des Francs, and **31**  
 498 A. Dereux, Generalized bloch equations for optical inter-  
 499 actions in confined geometries, *Chem. Phys. Lett.* **404**, 44  
 500 (2005). 501  
 502  
 [22] R. Kolesov, B. Grotz, G. Balasubramanian, R. J. Stöhr,  
 503 A. A. L. Nicolet, P. R. Hemmer, F. Jelezko, and J.  
 504 Wrachtrup, Wave-particle duality of single surface plasmon  
 505 polaritons, *Nat. Phys.* **5**, 470 (2009). **32** 506  
 507  
 [23] O. Mollet, S. Huant, G. Dantelle, T. Gacoin, and A. Drezet,  
 508 Quantum plasmonics: Second-order coherence of surface  
 509 495

- 496 plasmons launched by quantum emitters into a metallic film, *Phys. Rev. B* **86**, 045401 (2012). 532
- 497 [Phys. Rev. B 86, 045401 \(2012\)](#). 533
- 498 [24] M. Berthel, Q. Jiang, C. Chartrand, J. Belessa, S. Huant, C. 534
- 499 Genet, and A. Drezet, Coherence and aberration effects in 535
- 500 surface plasmon polariton imaging, *Phys. Rev. E* **92**, 536
- 501 [033202 \(2015\)](#). 537
- 502 [25] A. Drezet, Y. Sonnefraud, A. Cuche, O. Mollet, M. Berthel, 538
- 503 and S. Huant, Near-field microscopy with a scanning 539
- 504 nitrogen-vacancy color center in a diamond nanocrystal: 540
- 505 A brief review, *Micron* **70**, 55 (2015). 541
- 506 [26] B. Hecht, H. Bielefeldt, L. Novotny, Y. Inouye, and D. W. 542
- 507 Pohl, Local Excitation, Scattering, and Interference of 543
- 508 Surface Plasmons, *Phys. Rev. Lett.* **77**, 1889 (1996). 544
- 509 [27] A. Bouhelier, T. Huser, H. Tamaru, H. J. Güntherodt, 545
- 510 D. W. Pohl, F. I. Baida, and D. Van Labeke, Plasmon 546
- 511 optics of structured silver films, *Phys. Rev. B* **63**, 155404 547
- 512 (2001). 548
- 513 [28] A. Drezet, D. Koller, A. Hohenau, A. Leitner, F. R. 549
- 514 Aussenegg, and J. R. Krenn, Surface plasmon polariton 550
- 515 microscope with parabolic reflectors, *Opt. Lett.* **32**, 2414 551
- 516 (2007). 552
- 517 [29] A. Drezet and C. Genet, Imaging Surface Plasmons: From 553
- 518 Leaky Waves to Far-Field Radiation, *Phys. Rev. Lett.* **110**, 554
- 519 [213901 \(2013\)](#). 555
- 520 [30] A. Drezet, A. Hohenau, D. Koller, A. Stepanov, H. 556
- 521 Ditlbacher, B. Steinberger, F. R. Aussenegg, A. Leitner, 557
- 522 and J. R. Krenn, Leakage radiation microscopy of surface 558
- 523 plasmon polaritons, *Mater. Sci. Eng. B* **149**, 220 (2008). 559
- 524 [31] P. Bharadwaj, A. Bouhelier, and L. Novotny, Electrical 560
- 525 Excitation of Surface Plasmons, *Phys. Rev. Lett.* **106**, 561
- 526 [226802 \(2011\)](#). 562
- 527 [32] M. Berthel, S. Huant, and A. Drezet, Spatio-temporal 563
- 528 second-order quantum correlations of surface plasmon 564
- 529 polaritons, *Opt. Lett.* **41**, 37 (2016). 565
- 530 [33] H. Trung Dung, L. Knöll, and D.-G. Welsch, Spontaneous 566
- 531 decay in the presence of dispersing and absorbing bodies: 567
- General theory and application to a spherical cavity, *Phys. 568*
- Rev. A* **62**, 053804 (2000). 569
- [34] R. Carminati, M. Nieto-Vesperinas, and J. J. Greffet, Reciprocity of evanescent electromagnetic waves, *J. Opt. Soc. Am. A* **15**, 706 (1998). 570
- [35] E. R. Mendez, J.-J. Greffet, and R. Carminati, On the equivalence between the illumination and collection modes of the scanning near-field optical microscope, *Opt. Commun.* **142**, 7 (1997). 571
- [36] G. Colas des Francs, C. Girard, and A. Dereux, Theory of near-field optical imaging with a single molecule as light source, *J. Chem. Phys.* **117**, 4659 (2002). 572
- [37] N. Rotenberg, M. Spasenović, T. L. Krijger, B. le Feber, F. J. García de Abajo, and L. Kuipers, Plasmon Scattering from Single Subwavelength Holes, *Phys. Rev. Lett.* **108** 127402 (2012). 573
- [38] M. Berthel, O. Mollet, G. Dantelle, T. Gacoin, S. Huant, and A. Drezet, Photophysics of single nitrogen-vacancy centers in diamond nanocrystals, *Phys. Rev. B* **91**, 035308 (2015). 574
- [39] R. Beams, D. Smith, T. W. Johnson, S. H. Oh, L. Novotny, and A. N. Vamivakas, Nanoscale fluorescence lifetime imaging of an optical antenna with a single diamond NV center, *Nano Lett.* **13**, 3807 (2013). 575
- [40] G. Di Martino, Y. Sonnefraud, M. S. Tame, S. Kéna-Cohen, F. Dieleman, Ş. K. Özdemir, M. S. Kim, and S. A. Maier, Observation of Quantum Interference in the Plasmonic Hong-Ou-Mandel Effect, *Phys. Rev. Applied* **1**, 034004 (2014). 576
- [41] M.-C. Dheur, E. Devaux, T. W. Ebbesen, A. Baron, J.-C. Rodier, J.-P. Hugonin, P. Lalanne, J.-J. Greffet, G. Messin, and F. Marquier, Single-plasmon interferences, *Sci. Adv.* **2**, e1501574 (2016). 577
- [42] A. G. Curto, G. Volpe, T. H. Taminiau, M. P. Kreuzer, R. Quidant, N. F. van Hulst, Unidirectional emission of a quantum dot coupled to a nanoantenna, *Science* **329**, 930 (2010). 578